ELSEVIER

Thin Solid Films 411 (2002) 152–160

thin solid films

www.elsevier.com/locate/tsf

Combinatorial studies of Zn-Al-O and Zn-Sn-O transparent conducting oxide thin films

J.D. Perkins[a,*], J.A. del Cueto[a], J.L Alleman[a], C. Warmsingh[b], B.M. Keyes[a], L.M. Gedvilas[a], P.A. Parilla[a], B. To[a], D.W. Readey[b], D.S. Ginley[a]

[a]*National Renewable Energy Laboratory, SERF-E100-49, 1617 Cole Blvd, Golden CO, 80401-3393, USA*
[b]*Colorado School of Mines, Golden, CO, 80401, USA*

Abstract

In this work, we discuss the development of combinatorial deposition and analysis tools for the investigation of and the optimization of transparent conducting oxides. Library deposition by co-sputtering followed by optical analysis is shown to be a facile way to achieve these goals. Initial work focused on Zn-Al-O libraries with low Al contents as a test case. Subsequent work has focused on the ZnO-SnO_2 tie line. Local maxima in the composition dependence of the conductivity were found for Zn/Sn $\approx$2:1 (Zn_2SnO_4) and Zn/Sn $\approx$1:1 ($ZnSnO_3$). For these two representative stoichiometries, constant composition films have also been grown by pulsed laser deposition.

Keywords: Transparent conducting oxides; TCO; Combinatorial; Thin film

1. Introduction

Transparent conducting oxides play a key role in a number of thin film optoelectronic devices including flat panel displays, low-e windows, photovoltaics, electrochromic devices and anti-static coatings [1]. The bulk of these applications rely on the established n-type transparent conducting oxides (TCOs), such as SnO_2:F, ZnO:Al and Indium-Tin-Oxide (ITO) [2]. Next-generation devices will require improved or new TCOs [1]. In general, this drive for new materials is leading to the investigation of new 'exotic' n-type materials such as the binary metal oxide compounds Cd-Sn-O [3,4], Zn-In-O [5–8], Zn-Sn-O [4,9–11], Zn-Ga-O [12,13] and Ga-In-O [14–16]. These more complex materials are generally alloys of the simpler established transparent conducting metal oxides such as CdO, SnO_2, ZnO, In_2O_3 and Ga_2O_3 [17–19]. The compositional phase space spanned by these five simple metal oxides is quite large and contains many interesting materials. This is also leading to the current investigations of ternary metal compounds such as In-Sn-Zn-O [6,20–22], In-Ga-Zn-O [23,24], Ga-In-Sn-O [16,25,26], Cd-In-Sn-O [27–29] and Zn-Sn-Cd-O [4] which still represent only a small fraction of the more complex multinary compounds possible in this five dimensional composition space.

Furthermore, for these ternary metals studies, the stoichiometries examined are usually restricted to a small number of possibilities along carefully chosen tie lines joining known binary metal compounds. Hence, in order to facilitate more general ternary metal studies and perhaps even more complex quaternary studies, we have developed and are continuing to develop the deposition, characterization and analysis tools necessary to employ a combinatorial approach to thin film metal oxides with a special focus on transparent conducting oxides. In this work, we describe our combinatorial research [30] using Zn-Al-O as a test case and then report the current status of our on-going study of the Zn-Sn-O system. First, we note that the reported conductivities for Zn-Sn-O TCOs are quite low compared with well-known simple TCOs such as In_2O_3:Sn (ITO). In particular, for Zn_2SnO_4 $\sigma = 50-100\ \Omega^{-1}\text{-cm}^{-1}$ [18,31] and for $ZnSnO_3$ $\sigma = 250\ \Omega^{-1}\text{-cm}^{-1}$ [11] whereas for ITO $\sigma = 10^4\ \Omega^{-1}\text{-cm}^{-1}$ [2]. Nevertheless, our interest in Zn-Sn-O TCOs is threefold: First, Zn_2SnO_4 is an important interface layer in the CdS/CdTe world record polycrystalline solar cells (16.5% total-area efficiency) [9,32]; Second, $ZnSnO_3$ has a very high electron work function of 5.3 eV which

*Corresponding author. Tel.: +1-303-384-6606.
E-mail address: john_perkins@nrel.gov (J.D. Perkins).

0040-6090/02/$ - see front matter
PII: S0040-6090(02)00205-5

makes it attractive as a hole extracting electrode in polymer photovoltaics [18,33]; And third, Zn-Sn-O is a developmental step towards interesting multinary metal oxide systems such as Zn-Sn-In-O [6,20–22] and Zn-Sn-Cd-O [4].

2. Experimental approach

2.1. Combinatorial materials deposition

Compositionally varying combinatorial samples (libraries) can be deposited by a variety of techniques including PVD based (evaporation, sputtering, laser deposition), CVD based (MOCVD and PECVD) and solution based (sol–gel, inkjet). The materials deposition generally uses one of two different approaches to library generation, either continuous composition spread or multiple isolated discrete compositions. In the former method, the composition varies continuously over the entire library with composition gradients defined by source positions and relative fluxes. For the latter, the deposition method can be a continuous spread approach but with the sample masked to establish small areas with approximately constant composition or different deposition masks can be used for each different source in a sequential deposition approach. Alternatively, discrete composition array libraries can be made using a direct write deposition method such as ink jet printing where the mask is not required. We use a multi-gun sputtering system with either RF or DC capabilities to generate libraries with continuous composition gradients [30]. Both the substrate temperature and sputtering gas mixture, particularly the O_2 partial pressure, can be controlled with a maximum possible substrate temperature of $\sim$900 °C. In addition, ex-situ post-deposition anneals are done in flowing gas at ambient pressure using a tube furnace.

For the TCO libraries discussed here, we have co-sputtered from two targets of different composition onto glass substrates. The substrate size is either $2'' \times 2''$ or $3'' \times 3''$. This large substrate size enables easy analysis of many different spots (i.e. compositions). Our initial combinatorial deposition experiments have been on Al substituted ZnO. Subsequent experiments have focused on the ZnO-SnO_2 tie line. For these latter Zn-Sn-O libraries, the sputter sources are a ceramic ZnO target and a metallic Sn target. The ZnO target is always RF sputtered but the metallic Sn target is sputtered using either RF or DC mode. The substrate temperature is 250 °C during deposition and the libraries are generally post-deposition annealed ex-situ in flowing N_2 at temperatures ranging from 400 to 700 °C.

2.2. Combinatorial materials characterization

For a combinatorial approach to be effective, the characterization, data analysis, and data reduction throughput must match the deposition throughput. Otherwise, the resultant analysis bottleneck will result in a huge back log of unanalyzed samples and the value of the combinatorial deposition will be largely eliminated. This requires the development of appropriate characterization tools, which must be position scanable and highly automated with rapid data acquisition and analysis. In addition, appropriate data analysis tools, data basing tools and data mining tools must be developed in order to extract useful material science and optimization information from the very large amounts of raw data that automated characterization of combinatorial libraries creates. At present, in this area, we have improved the measurement throughput and automation by developing high throughput characterization tools but are just beginning to work on high throughput data analysis as well as data basing and data mining strategies. For the specific area of TCOs, it appears, at present, that conductivity mapping coupled with optical characterization (UV/Vis/NIR) and metals-composition analysis is sufficient for initial screening of the libraries. Subsequent phase identification by X-ray diffraction (XRD) and electronic structure information by X-ray photoelectron spectroscopy (XPS) may be necessary once interesting areas in phase space are identified.

The work for TCO library characterization focuses on the development of optical characterization tools. There are three main reasons for this: First, for TCOs, the optical properties are a critical performance parameter; Second, many optical techniques are inherently non-contact and hence amenable to automated scanning; and third, it appears that proper modeling of the optical data can yield relevant structural and electronic information such as the local film thickness and the carrier concentration.

3. Results and discussion

3.1. Optical characterization (UV/VIS/NIR)

Fig. 1 shows the optical transmission spectrum for five representative elements of a Zn(Al)O library which was deposited by co-sputtering from ZnO and Al targets. These spectra are measured using a UV/VIS/NIR CCD-based fiber-optically-coupled spectrometer. For each spectrum shown in Fig. 1, the data acquisition time is less than one second for the full spectrum. These short acquisition times, which are critical for automated combinatorial analysis, are possible since the CCD array based spectrometer measures the transmission at all wavelengths simultaneously. By using a split collection fiber and two separate spectrometer channels, the full spectral range that can be acquired simultaneously is 200–1100 nm. In the near future, this will be extended to 2200 nm by using a third channel with an extended-response InGaAs based detector array.

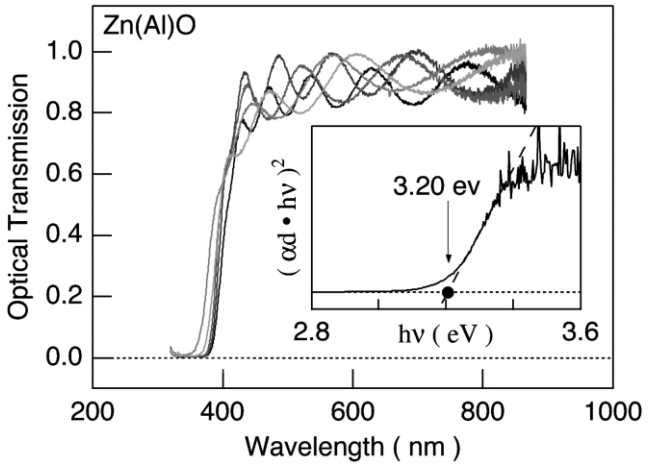

Fig. 1. Optical transmission spectra of 5 representative elements of a sputtered Zn(Al)O library.

From optical transmission spectra such as shown in Fig. 1, one can determine the optical band gap from the short wave-length cut off of the transmission as well as the film thickness and the index of refraction from the spacing and magnitude of the interference fringes at wavelengths longer than the band gap. The inset in Fig. 1 shows the determination of the band gap energy for a direct-band-gap optically allowed transition as appropriate for zinc oxide. For the spectra shown, the resultant band gap is 3.2 eV. The oscillating optical transmission seen in Fig. 1 for wave-lengths between 600 and 900 nm is due to interference among multiple internal reflections within the film. Assuming no absorption in the film over the spectral range of interest, these interference fringes depend only upon the film thickness, the index of refraction for the film and the index of refraction of the substrate. Assuming a constant index of refraction for both the film and the substrate, the wavelength dependant transmission normalized to that of a bare substrate is given by

$$\tilde{T}=\frac{T}{T_{\text{glass}}}=\frac{\left(\frac{n_g+1}{n+1}\right)^2\left(\frac{2n}{n+n_g}\right)^2}{1+\left(\frac{n-1}{n+1}\right)^2\left(\frac{n-n_g}{n+n_g}\right)^2-2\left(\frac{n-1}{n+1}\right)\left(\frac{n-n_g}{n+n_g}\right)\cos\left(2\pi\left(\frac{2nd}{\lambda}\right)\right)} \quad (1)$$

where n is the film index of refraction, n_g, the substrate index of refraction, d, the film thickness and λ, the wavelength of light. Using this equation to fit the data, one can determine both the film thickness and the film index of refraction in the zero absorption region.

An example is shown in Fig. 2. The fit works well and the fit-determined film thickness is ~6000 Å in good agreement with the thickness measured using conventional step profilometer measurements. Extending the spectral range of the measurements to 2200 nm, which is planned, will improve this analysis by allowing the measurement of more fringes. For thinner films, the fringes broaden making the optical determination of the film thickness less reliable. Also, simultaneous measurement and fitting of both the optical reflection and transmission spectra will enable improved determination of the infrared index of refraction and the absorption.

3.2. Optical characterization (FTIR)

For transparent conducting oxides, the decrease in the optical transmission in the infrared is due to collective plasma oscillations of the conducting electrons. At longer wavelengths, this yields a marked increase in the reflectivity. The cross over from transmitting to reflecting behavior with increasing wavelength depends upon the conducting electron density, N, and occurs at the plasma frequency, ω_p, given by

$$\omega_p=\sqrt{\frac{4\pi Ne^2}{\varepsilon_\infty m^*}} \quad (2)$$

which means that the plasma wavelength, λ_p, goes roughly as

$$\lambda_p\sim\sqrt{\frac{m^*}{N}} \quad (3)$$

So, as the carrier concentration, and hence usually the conductivity, are increased, the plasma edge moves to shorter wavelengths. For a combinatorial approach, this also means that optical measurements of the plasma frequency can be used as a non-contact probe to measure the relative carrier concentration.

Fig. 3 shows the infrared reflectivity vs. photon energy (8065 $cm^{-1}=1$ eV). The SnO_2 reference sample shows the increase in reflectance at low energy (long

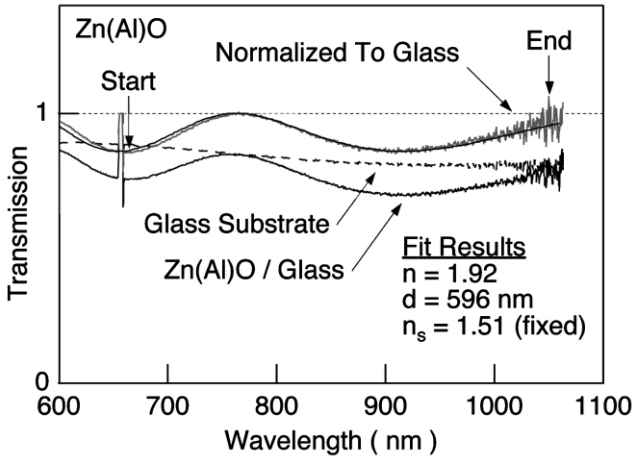

Fig. 2. Fit to optical transmission data to determine film thickness and index of refraction.

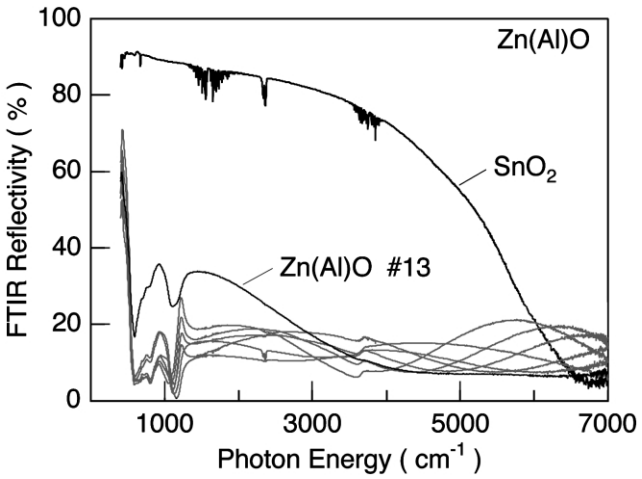

Fig. 3. FTIR reflectivity analysis of representative elements of a Zn(Al)O library.

wavelength) typical of good TCOs. The other spectra shown are for representative elements of the Zn(Al)O library from Fig. 1. Only one spectra, that for element 13, shows any sign of free carrier infrared reflection. Using a linear 4-point transport measurement, the conductivity, σ, of element 13 is 40 Ω^{-1}-cm^{-1} whereas for all of the other elements, $\sigma \leq 7$ Ω^{-1}-cm^{-1}.

Using gray scale intensity maps, Fig. 4 summarizes several properties of a recent Zn(Al)O library. The upper left map shows the infrared reflectance at a photon energy of 2000 cm^{-1}. While a line shape fit to determine the plasma frequency from the reflectance spectra would be best [3,30], we find that, for any given library, the simple reflectance at a characteristic library-specific photon energy is generally sufficient to determine the region of highest carrier concentration [30]. For this Zn(Al)O library, the 2000 cm^{-1} reflectance map indicates a higher electron density on right side of the sample than the left with a weaker increase from the top to the bottom. This is quite reasonable, since the Al sputtering gun, which supplies the electron-donating Al,

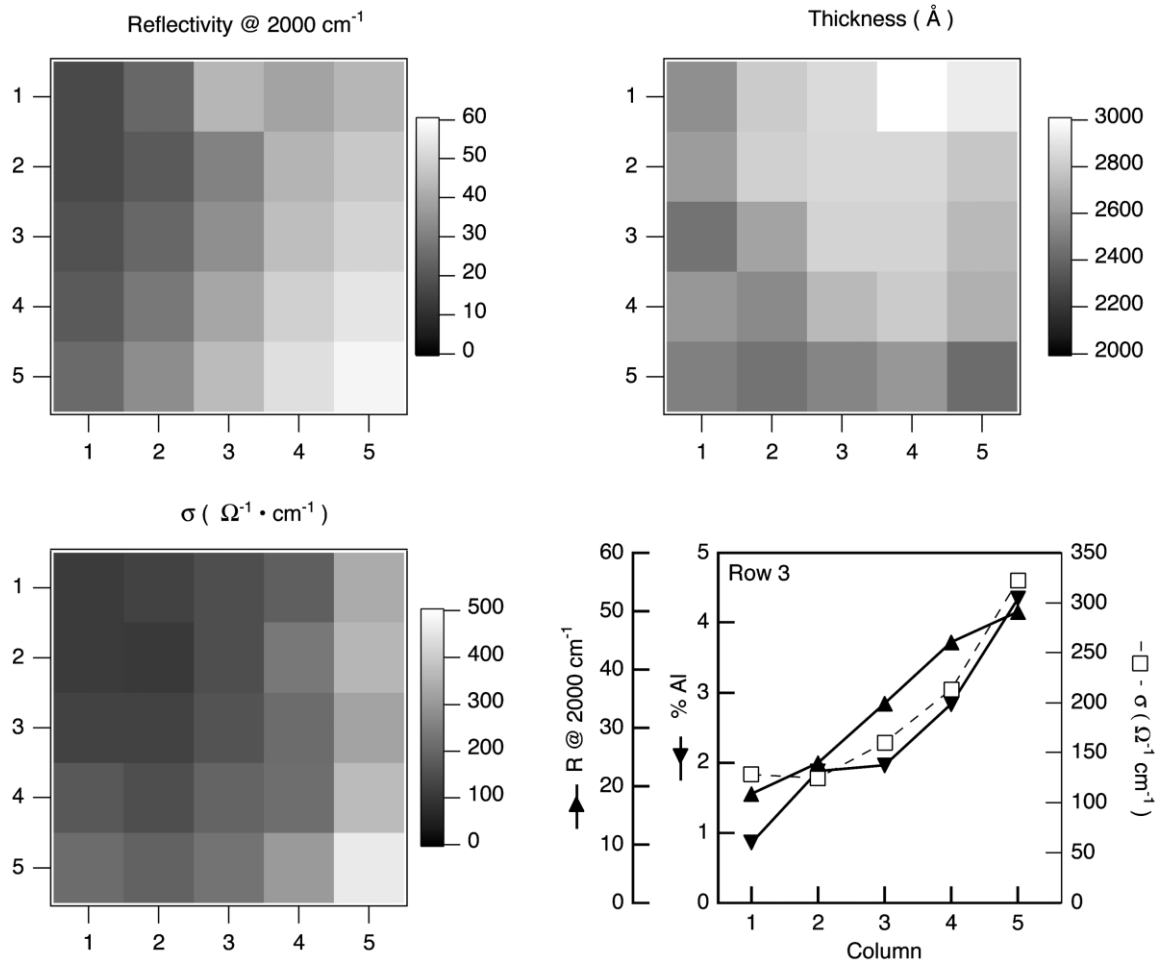

Fig. 4. Gray scale intensity maps of relevant materials properties by element position within a sputtered Zn(Al)O library.

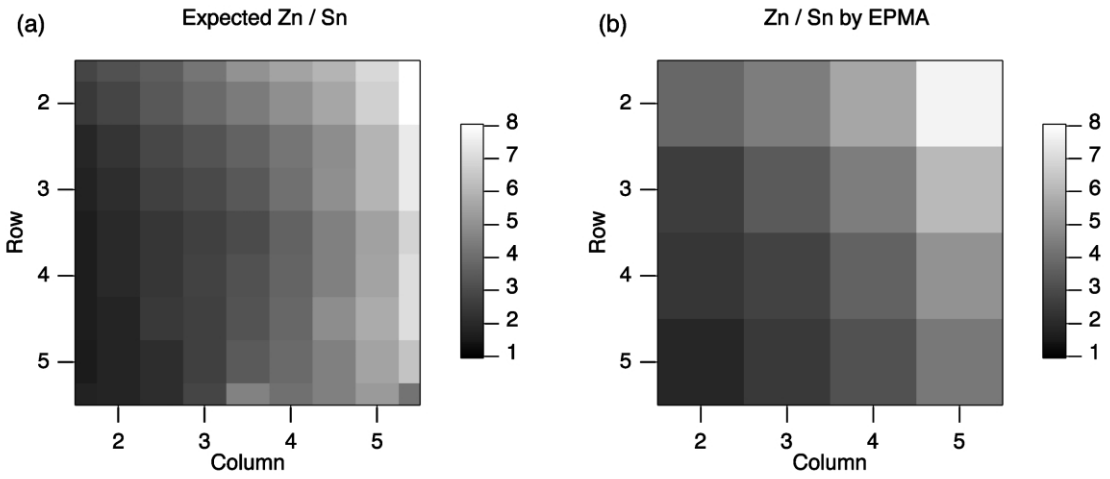

Fig. 5. Gray scale intensity maps of expected (left) and actual (right) Zn/Sn metals ratio in co-sputtered Zn-Sn-O combinatorial library.

is on the right side of the substrate. The thickness map in the upper right shows that the thickness is between 2000 and 3000 Å which we consider to be reasonably uniform given that the substrate is large (3″×3″) and the main ZnO sputtering target is 2″ in diameter. Using this thickness information, measured using profilometry, and the sheet resistance, measured using a linear four point probe, one can get the bulk conductivity map shown in the bottom left. We note that within this map, the right edge is more conducting in accord with expectations from the infrared reflectivity map. The bottom right graph shows the conductivity (□, right axis), infrared optical reflectance at 2000 cm^{-1} (▲, auxiliary left axis) and the relative aluminum content (▼, main left axis), measured using electron microprobe, vs. column position for row 3. For this sample, the conductivity generally scales with Al content. In particular, for the right most element of column 3, $\sigma = 320$ Ω^{-1}-cm^{-1} and for the bottom right corner-element, $\sigma = 460$ Ω^{-1}-cm^{-1}. While this is just the well-expected result [2], it demonstrates the both validity of the co-sputtering approach to combinatorial library deposition combinatorial analysis tools. No further work was done on Zn-Al-O libraries since our primary reason for working with this well studied material system was as a test case for combinatorial technique and system development.

3.3. Sputter deposited Zn-Sn-O libraries

Based on the recent results for CdS/CdTe solar cells [9] and other recent work [4] there is considerable interest in the Zn-Sn-O family of transparent conductors. Furthermore, a combinatorial study of the binary metal oxide ZnO-SnO_2 tie line will be a good developmental step towards combinatorial studies of the related ternary metal oxide systems such as Zn-Sn-In-O [20,21] and Zn-Sn-Cd-O [4]. Unlike the case of Al doped ZnO, where the Al contents of interest are 5 at.% or less, the interest in the Zn-Sn-O system spans the full compositional space from ZnO to SnO_2.

Using gray scale intensity maps, Fig. 5 shows the Zn/Sn metals stoichiometry for one Zn-Sn-O library as co-sputtered from ZnO and Sn-metal targets with both sputtering guns using RF power. The metals ratio was measured using EPMA (electron microprobe) as referenced to a Zn_2SnO_4 thin film reference sample, which had been previously characterized by Rutherford backscattering (RBS). The left map in Fig. 5 shows the 'expected' Zn/Sn ratio as determined by using a linear superposition of the individual, independently measured, ZnO and SnO_2 deposition rate maps. For this library, the expected Zn/Sn ratio ranges from ~ 2 in the lower left corner to ~ 8 in the upper right corner. The right map shows the measured Zn/Sn ratio using the same gray scale. Comparing these two maps, both the composition range and the spatial dependence of the composition are very similar, indicating that, to a large extent, the Zn and Sn sputtering rates are independent and comparable to those in the calibration runs.

Fig. 6 shows the conductivity before and after annealing for this Zn-Sn-O library. These two maps show the gray scale intensity map of the conductivity on a logarithmic scale. Note that the full gray scale goes -5 to $+2$, a seven order of magnitude range for the conductivity. On this large scale, the left hand map for the as-deposited library is quite uniform in gray shade with the conductivity $\sigma = 10^{-2}$ to 10^{-1} Ω^{-1}-cm^{-1} ($\log(\sigma) = -2$ to -1 in the figure) whereas the right hand map for the post-annealed library spans the entire gray scale indicating a seven order of magnitude variation of the conductivity in this library from $\sigma = 10^{-5}$ to 10^{+2} Ω^{-1}-cm^{-1}. Note that, in comparison with the as-deposited conductivity map, annealing both increases the conductivity by three orders of magnitude for some

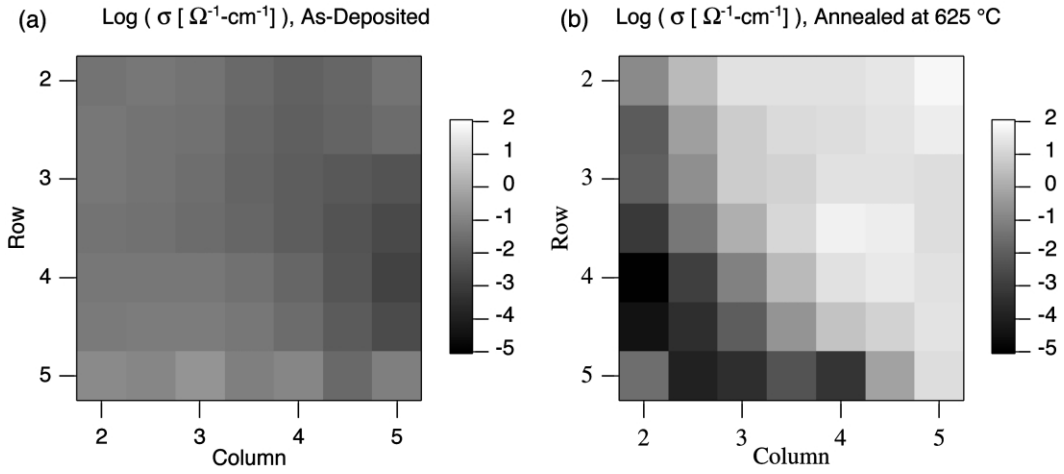

Fig. 6. Logarithmic gray scale intensity maps of the conductivity for as-deposited (left) and annealed (right) Zn-Sn-O libraries. The gray scale range is the same for both maps.

regions of the library and decreases the conductivity by three orders of magnitude for other regions of the library. This library was annealed in flowing N_2 at 625 °C. Comparison of the maps in Figs. 5 and 6 shows that the directions of the composition and conductivity gradients are well aligned suggesting that the spatial variation of the Zn/Sn ratio accounts for the varying conductivity.

Fig. 7 shows X-ray diffraction (XRD) θ/2θ spectra for two representative points on this Zn-Sn-O library. The measured Zn/Sn map from Fig. 5 is included as an inset. The top XRD spectrum was taken at the location indicated by the circle in the inset where Zn/Sn ∼2. All lines in this XRD spectrum are well accounted for by randomly-oriented crystalline Zn_2SnO_4. The bottom XRD spectrum was taken at the location indicated by the triangle in the inset where Zn/Sn ∼7. The one weak XRD line seen aligns well with that for (002) oriented ZnO, which is a common orientation for ZnO thin films on glass. Hence, given the weak XRD crystallinity and the high Zn/Sn ratio, this region is likely best described as heavily Sn substituted ZnO.

Fig. 8 shows the UV/VIS optical transmission spectra for two representative locations on the Zn-Sn-O library. Again the Zn/Sn map is included as an inset with a circle indicating the Zn/Sn ∼2 location and a triangle

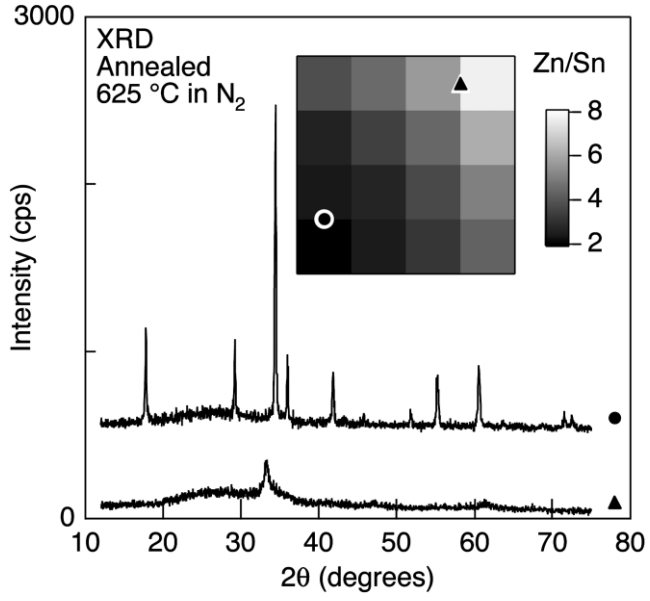

Fig. 7. Main panel: XRD θ/2θ spectra library elements with Zn/Sn ∼7 (triangle) and Zn/Sn ∼2 (circle). Inset: Gray scale intensity map for Zn/Sn ratio indicating the measurement locations for the two XRD spectra shown.

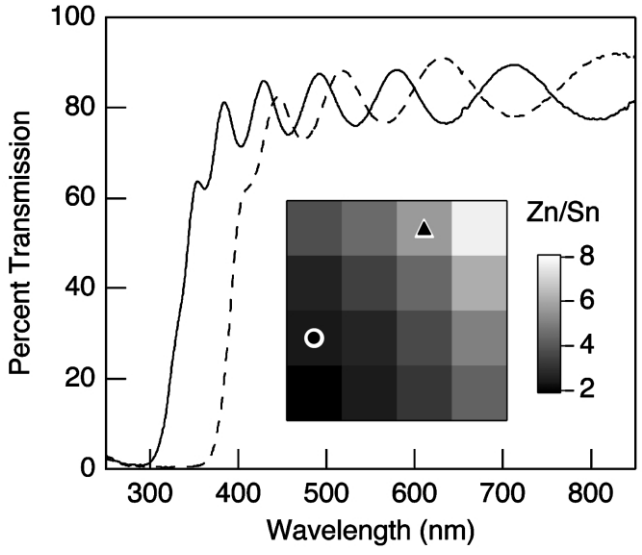

Fig. 8. Main panel: UV/VIS optical transmission spectra library elements with Zn/Sn ∼6 (triangle, dashed line) and Zn/Sn ∼2 (circle, solid line). Inset: Gray scale intensity map for Zn/Sn ratio indicating the measurement locations for the two spectra shown.

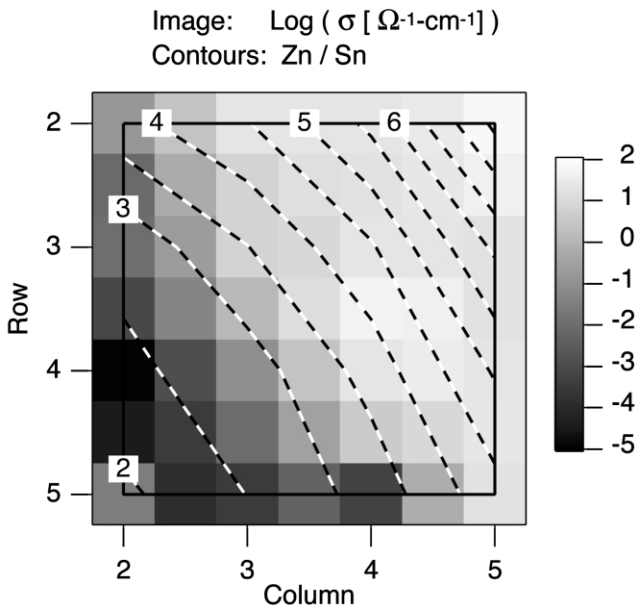

Fig. 9. Superposition of logarithmic gray scale intensity conductivity map and linear contour composition map for Zn-Sn-O library with $2 < Zn/Sn < 8$.

indicating the Zn/Sn ~6 location. The two measured optical spectra show that the band gap for the Zn_2SnO_4 region (lower left) occurs at shorter wavelengths than that for the ZnO region (upper right).

For this Zn-Sn-O library, the property maps shown in Fig. 5 through 8 strongly suggest that the dominant controlling variable is, as intended, the Zn/Sn cation ratio. To make this clearer, in Fig. 9 we overlay the conductivity map for the annealed library from Fig. 6 and the measured Zn/Sn cation ratio map from Fig. 5. In Fig. 9, the conductivity is shown using a gray scale intensity map with a logarithmic scale and the Zn/Sn ratio is shown using a contour map. The contour interval is 0.5 and the contours for Zn/Sn = 2, 3, 4, 5 and 6 are labeled. Overall, there is a very clear correlation between the Zn/Sn ratio and the conductivity after annealing at 625 °C in flowing N_2.

In Fig. 10 we show a similar map for another library with overlaid post-annealing conductivity and Zn/Sn maps plotted in the same way. However, for this library, the Zn/Sn ratio varies from slightly less than one to approximately three. The contour interval for the Zn/Sn map is 0.2 in this case and the contours for Zn/Sn = 1 and 2 are labeled. For this library, again the metals composition map and the conductivity map are well correlated. For this library, the most conducting region is for Zn/Sn ~2 with $\sigma = 10^{-1}$ Ω^{-1}-cm^{-1}. However, there is a second local maximum in the conductivity for Zn/Sn ~1 with $10^{-2} < \sigma < 10^{-1}$ Ω^{-1}-cm^{-1} although there is noticeable scatter in the conductivity along the Zn/Sn = 1 contour. This latter observation was unexpected and compositionally Zn/Sn = 1 could correspond to the known $ZnSnO_3$ phase [11]. To date, there has only been a small amount of work on applications of $ZnSnO_3$ as a TCO. As a result of the combinatorial results shown in Fig. 10, we have an increased interest in $ZnSnO_3$ as TCO and its possible use in solar cell applications [9].

3.4. Pulsed laser deposition (PLD) deposited Zn_2SnO_4 and $ZnSnO_3$

To further study regions of interest as identified by the combinatorial results discussed above, thin film samples were grown by pulsed laser deposition (PLD) from Zn_2SnO_4 and $ZnSnO_3$ ceramic targets. This PLD system and its general application to mixed metal oxide film growth has been previously described [34,35]. For these TCO depositions, the films were deposited using a KrF laser operating at 248 nm with a 300 mJ/pulse at 10 Hz. The target to substrate distance was ~8 cm and the oxygen partial pressure during deposition was 5 millitorr. Fig. 11 shows the XRD $\theta/2\theta$ spectra for a film grown from the Zn_2SnO_4 target as well as that for a blank glass substrate. Note that crystalline XRD peaks, which correspond to (111)-textured Zn_2SnO_4, are just beginning to appear in the spectrum. This film was annealed in vacuum after deposition in the PLD chamber itself. The resultant conductivity is 17 Ω^{-1}-cm^{-1}, the best to date for our PLD-deposited Zn_2SnO_4 films. Films annealed at higher temperatures show much stronger crystalline XRD scattering corresponding to both textured and randomly-oriented Zn_2SnO_4, but they are not as conducting. PLD deposited films annealed at

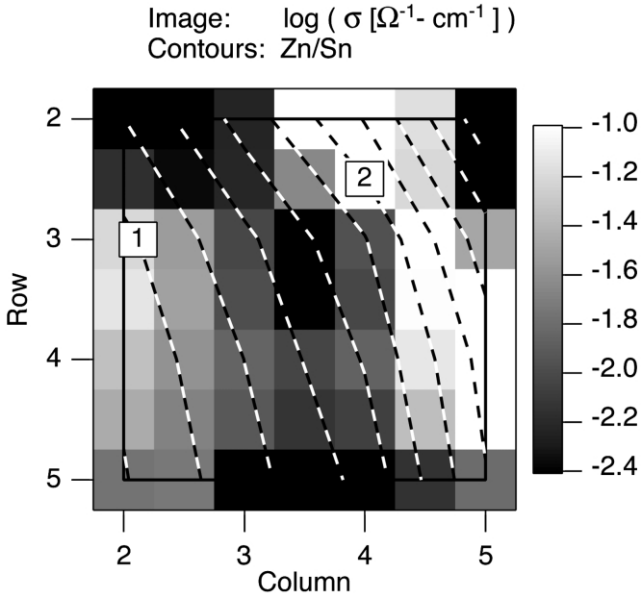

Fig. 10. Superposition of logarithmic gray scale intensity conductivity map and linear contour composition map for Zn-Sn-O library with $1 < Zn/Sn < 3$.

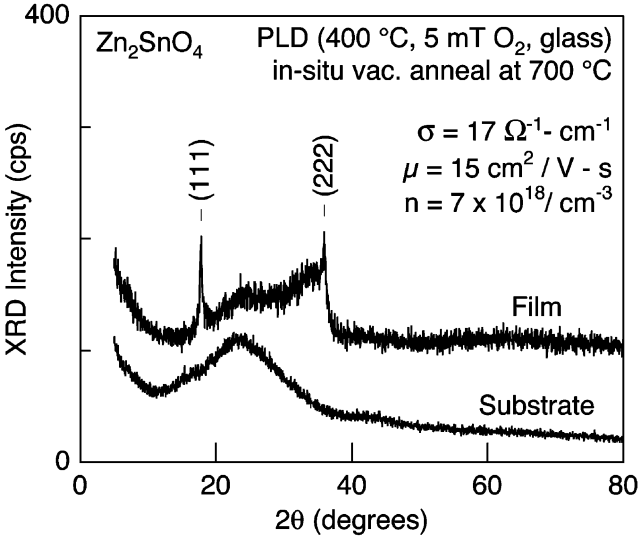

Fig. 11. XRD θ/2θ spectra for conducting Zn_2SnO_4 film grown by pulsed laser deposition. Spectra are shown for both the film and the bare glass substrate.

650 °C are amorphous showing no crystalline XRD scattering.

Fig. 12 shows the XRD θ/2θ spectrum for a PLD-deposited film grown from the $ZnSnO_3$ target. No sharp XRD lines are observed indicating that this film grown at 500 °C in 5 millitorr of O_2 is amorphous. For films grown by PLD from the $ZnSnO_3$ target, this is the highest substrate temperature used to date and no annealing experiments have been done yet. With mobility $\mu =$ 33 cm^2/V-s and carrier concentration $n = 3.5 \times 10^{19}$/ cm^3, the conductivity, 54 Ω^{-1}-cm^{-1}, for this film is better than that for the Zn_2SnO_4 film of Fig. 11 and markedly higher than that for the Zn/Sn = 1 region of the combinatorial library shown in Fig. 10. For a similar PLD-grown $ZnSnO_3$ film deposited at 400 °C in 1 millitorr of O_2, the conductivity as-deposited is 200 Ω^{-1}-cm^{-1} with a mobility $\mu = 35$ cm^2/V-s and $n = 3.5 \times 10^{19}/cm^3$. Thus, the early results for PLD grown $ZnSnO_3$ films indicate that the Zn/Sn ~1 region initially identified by the combinatorial approach continues to show promise for photovoltaic applications [9]. More detailed experiments are in progress to further study this region as well as to further compare the combinatorial sputter-deposited libraries with the single-composition PLD-deposited films.

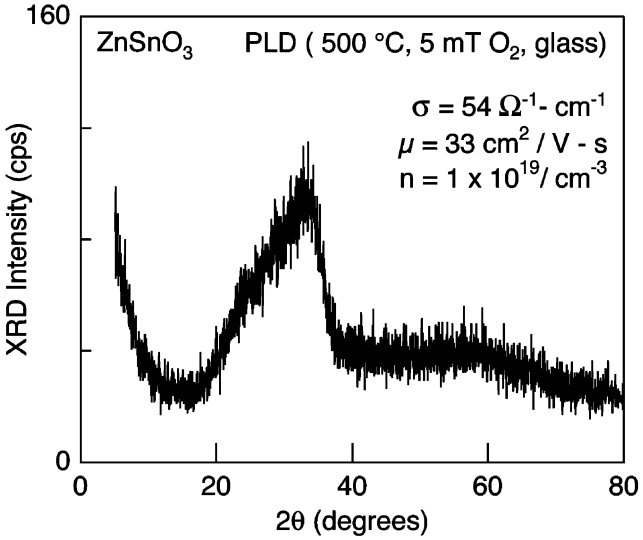

Fig. 12. XRD θ/2θ spectra for conducting $ZnSnO_3$ film grown by pulsed laser deposition.

4. Summary

In this work, we have discussed the development of combinatorial deposition and analysis tools for the investigation and optimization of transparent conducting oxides. Library deposition by co-sputtering followed by optical analysis has proven a facile way to achieve this goal. Initial developmental work focused on Zn-Al-O libraries with small Al content as a test case. Subsequent work focused on the ZnO-SnO_2 tie line. Local maxima in the composition dependence of the conductivity were found for Zn/Sn ≈ 2:1 (Zn_2SnO_4) and Zn/Sn ≈1:1 ($ZnSnO_3$). For these two representative stoichiometries, subsequent pulsed laser deposition film growth of constant composition films confirmed the potential interest of both compositions for photovoltaic applications.

Acknowledgments

This work was supported by the US Department of Energy under Contract no. DE-AC36-99-GO10337 through the NREL DDRD program.

References

[1] D.S. Ginley, C. Bright, MRS Bull. 25 (2000) 15.
[2] R.G. Gordon, MRS Bull. 25 (2000) 52.
[3] T.J. Coutts, D.L. Young, X. Li, MRS Bull. 25 (2000) 58.
[4] T.J. Coutts, D.L. Young, X. Li, W.P. Mulligan, X. Wu, J. Vac. Sci. Technol. A 18 (2000) 2646.
[5] T. Minami, H. Sohohara, T. Kakumu, S. Takata, Jpn. J. Appl. Phys. Part 2-Lett 34 (1995) L971.
[6] J.M. Phillips, R.J. Cava, G.A. Thomas, S.A. Carter, J. Kwo, T. Siegrist, J.J. Krajewski, J.H. Marshall, W.F. Peck, D.H. Rapkine, Appl. Phys. Lett. 67 (1995) 2246.
[7] T. Minami, H. Kumagai, T. Kakumu, S. Takata, M. Ishii, J. Vac. Sci. Technol. A 15 (1997) 1069.
[8] H. Hiramatsu, W.S. Seo, K. Koumoto, Chem. Mater. 10 (1998) 3033.
[9] X. Wu, S. Asher, D.H. Levi, D.E. King, Y. Yan, T.A. Gessert, P. Sheldon, J. Appl. Phys. 89 (2001) 4564.
[10] D.L. Young, T.J. Coutts, D.L. Williamson, Mater. Res. Soc. Symp. Proc. 666 (2001) F3.8.
[11] T. Minami, H. Sohohara, S. Takata, H. Sato, Jpn. J. Appl. Phys. Part 2 33 (1994) L1693.

[12] T. Omata, N. Ueda, K. Ueda, H. Kawazoe, Appl. Phys. Lett. 64 (1994) 1077.
[13] Y.E. Lee, D.P. Norton, J.D. Budai, Y. Wei, J. Appl. Phys. 90 (2001) 3863.
[14] R.J. Cava, J.M. Phillips, J. Kwo, G.A. Thomas, R.B. Dover, S.A. Carter, J.J. Krajewski, W.F. Peck, J.H. Marshall, D.H. Rapkine, Appl. Phys. Lett. 64 (1994) 2071.
[15] J.M. Phillips, J. Kwo, G.A. Thomas, S.A. Carter, R.J. Cava, S.Y. Hou, J.J. Krajewski, J.H. Marshall, W.F. Peck, D.H. Rapkine, R.B. van Dover, Appl. Phys. Lett. 65 (1994) 115.
[16] D.D. Edwards, T.O. Mason, J. Am. Ceram. Soc. 81 (1998) 3285.
[17] A.J. Freeman, K.R. Poeppelmeier, T.O. Mason, R.P.H. Chang, T.J. Marks, MRS Bull. 25 (2000) 45.
[18] T. Minami, MRS Bull. 25 (2000) 38.
[19] H. Kawazoe, K. Ueda, J. Am. Ceram. Soc. 82 (1999) 3330.
[20] G.B. Palmer, K.R. Poeppelmeier, T.O. Mason, Chem. Mater. 9 (1997) 3121.
[21] G.B. Palmer, K.R. Poeppelmeier, T.O. Mason, J. Solid State Chem. 134 (1997) 192.
[22] T. Minami, T. Kakumu, K. Shimokawa, S. Takata, Thin Solid Films 371 (1998) 318.
[23] T. Moriga, D.R. Kammler, T.O. Mason, G.B. Palmer, K.R. Poeppelmeier, J. Am. Ceram. Soc. 82 (1999) 2705.
[24] M. Orita, H. Ohta, M. Hirano, S. Narushima, H. Hosono, Philos. Mag. B-Phys. Condens. Mater Stat. Mech. Electron. 81 (2001) 501.
[25] D.D. Edwards, T.O. Mason, F. Goutenoire, K.R. Poeppelmeier, Appl. Phys. Lett. 70 (1997) 1706.
[26] D.D. Edwards, T.O. Mason, W. Sinkler, L.D. Marks, K.R. Poeppelmeier, Z. Hu, J.D. Jorgensen, J. Solid State Chem. 150 (2000) 294.
[27] D.R. Kammler, T.O. Mason, D.L. Young, T.J. Coutts, J. Appl. Phys. 90 (2001) 3263.
[28] D.R. Kammler, T.O. Mason, K.R. Poeppelmeier, J. Am. Ceram. Soc. 84 (2001) 1004.
[29] L.N. Brewer, D.R. Kammler, T.O. Mason, V.P. Dravid, J. Appl. Phys. 89 (2001) 951.
[30] J.D. Perkins, D.W. Readey, J.L. Alleman, J.A. del Cueto, X. Li, T.J. Coutts, R.E. Stauber, C. Duncan, D.L. Young, P.A. Parilla, B.M. Keyes, L. Gedvilas, D. Balzar, Q. Wang, D.S. Ginley, Mater. Res. Soc. Symp. Proc. 666 (2001) F1.6.
[31] D.L. Young, D.L. Williamson, T.J. Coutts, J. Appl. Phys. 91 (2002) 1464.
[32] X. Wu, R.G. Dhere, D.S. Albin, T.A. Gessert, C. DeHart, J.C. Keane, A. Duda, T.J. Coutts, S. Asher, D.H. Levi, H.R. Moutinho, Y. Yan, T. Moriarty, S. Johnston, K. Emery, P. Sheldon, NCPV Program Review Proceedings (2001) 47.
[33] T. Minami, T. Miyata, T. Yamamoto, Surf. Coat. Technol. 108–109 (1998) 583.
[34] J.M. McGraw, J.D. Perkins, F. Hasoon, P.A. Parilla, C. Warmsingh, D.S. Ginley, E. Mateeva, D.W. Readey, J. Mater. Res. 15 (2000) 2249.
[35] J.D. Perkins, C.S. Bahn, J.M. McGraw, P.A. Parilla, D.S. Ginley, J. Electrochem. Soc. 148 (2001) A1302.